Exploring a Database of Optimal Airfoils for Axial Compressor Design

Markus Schnoes and Eberhard Nicke
markus.schnoes@dlr.de

German Aerospace Center (DLR)
Institute of Propulsion Technology
51147 Cologne, Germany

ABSTRACT

Ensuring a high degree of commonality among a range of products can dramatically decrease development costs. This paper aims to generate a highly versatile compressor airfoil family that covers most applications in the core compression system of aircraft engines and stationary gas turbines. This airfoil family is generated by filling a database with optimized airfoil shapes. The database is structured in seven dimensions, denominated as "design requirements": blade stagger angle, pitch-chord ratio, profile area and the following design point properties: inlet Mach number, Reynolds number, streamtube contraction and aerodynamic loading. Additional constraints are imposed to ensure that feasible airfoils exist for each set of requirements. These constraints include limitations for profile area depending on inlet Mach number and limits for axial Mach number.

To fill this seven-dimensional space, a large number of airfoils is generated by means of numerical optimization at discrete points in this space. The target is to find airfoil shapes that have low losses and ensure stable operation over wide incidence ranges. Design and off-design performance is evaluated with the blade-to-blade flow solver MISES. To verify the optimization strategy, it is tested on a set of existing compressor airfoils. The optimized geometries of four of the airfoils under investigation are found in the appendix.

The database offers a wide variety of airfoils for different applications. Airfoils for sub- and supersonic inflow are covered as well as airfoils suited for placement at hub or casing. The benefit of using airfoils optimized for their specific purpose over having generic airfoil shapes is discussed as well. In future, this airfoil database will be used to study novel concepts for aircraft engines.

NOMENCLATURE

Acronyms

RANS	Reynolds-averaged Navier-Stokes

Greek letters

β	relative flow angle measured from circumferential direction
ω	total pressure loss coefficient
$\overline{\omega}$	average total pressure loss coefficient
ρ	density
γ	blade stagger angle

Latin letters

a	profile area relative to squared chord length
WR	working range in degree of inlet flow angle
c	blade chord length
DF	diffusion factor
f	objective function
M	Mach number
MVDR	$= (\rho_2 \mathrm{v}_{\mathrm{m},2})/(\rho_1 \mathrm{v}_{\mathrm{m},1})$, meridional velocity density ratio
Re	Reynolds number
s	blade pitch
v	velocity

Sub- and superscripts

90	quantity of 90% working range
1	cascade inlet quantity
2	cascade outlet quantity
$*$	quantity at minimum loss
ch	near choke operating point
dp	design operating point
m	meridional direction
st	near stall operating point
θ	circumferential direction

INTRODUCTION

While gas turbines work at part-speed and part-load, compressor airfoils operate over a wide range of inlet Mach numbers and incidence. The aerodynamic quality of an airfoil is characterized by its losses and width of operation range while a defined loading requirement has to be fulfilled at a prescribed design point. Improving airfoil shape is strongly connected to the advancement in overall compressor design. Airfoil design has a long history starting in the beginning of the last century with systematic investigations on airfoil shape in wind tunnel tests. For the following decades airfoil series like NACA-65 or double-circular-arc (DCA) blades defined the state-of-the-art [1, 2] in compressor design. In the 1980s, controlled diffusion airfoils presented by Hobbs et al.[3] emerged. Based on an interactive computer design system, these airfoils offer shock-free flow at high subsonic inlet Mach numbers increasing the range of operation significantly. In the 1990s, Köller et al. [4, 5] employed direct numerical optimization in combination with the blade-to-blade flow solver MISES to generate a set of optimal profile geometries for systematically varying cascade properties. These airfoils have been specifically optimized for wide incidence ranges by calculating multiple operating points for each candidate geometry.

In [6] the ideas of Köller have been adopted and a database of optimal airfoils was presented together with methods to access optimal airfoil shape and perfor-

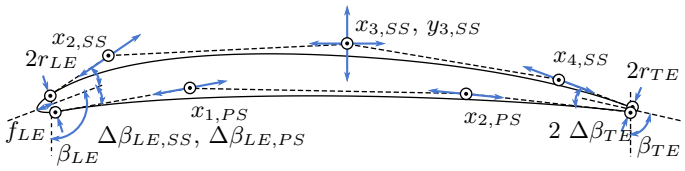

Figure 1: Design parameters describing airfoil geometry (parameters not included in nomenclature)

mance. On this basis two subsonic stages of a research compressor have been redesigned with database airfoils in a throughflow setup. Computations with 3D CFD confirmed the capabilities to increase efficiency and stability margin.

Airfoils presented both in [4] and [6] are limited to subsonic inflow. This work refines the strategies presented in [6] and extends the application to cascades with supersonic inflow and adds dependencies on MVDR and Reynolds number. The airfoil family in this work is structured in seven dimensions, denominated as "design requirements": stagger angle γ, pitch-chord ratio $\frac{s}{c}$ and cross-sectional area a, together with the design point properties inlet Mach number M_1, Reynolds number Re, streamtube contraction MVDR and aerodynamic loading based on the diffusion factor DF^{dp}. The diffusion factor DF is defined as:

$$DF = 1 - \frac{v_2}{v_1} + \frac{v_{1,\theta} - v_{2,\theta}}{2v_1}\frac{s}{c}. \tag{1}$$

As no prior knowledge is available on the range of flow turning for the optimized airfoil shapes, the design point diffusion factor is used as parameter defining aerodynamic loading.

This text begins by introducing the reader to the design tools and continues by presenting the optimization strategy. Afterwards, the creation of the database of optimized airfoils is outlined. To verify the quality of the new airfoils, the performance of two candidates is compared to RANS calculations. Two additional airfoils are compared to a controlled diffusion airfoil and a state-of-the-art profile by Köller [4]. The geometry of the four optimized airfoil shapes under investigation is found in the appendix.

DESIGN METHODS

The airfoil design process is based on tools for geometry generation, blade-to-blade flow simulation and numerical optimization.

Airfoil geometry generation

The in-house program "BladeGenerator" is used to define a parametric description of the blade shape. Suction and pressure side are constructed with cubic B-splines and leading and trailing edge are appended. The shape parameters are presented in Fig. 1. A high degree of freedom is assured by using five control points for the suction side and four control points for the pressure side. Leading and trailing edge shape are defined by their radius and additionally the leading edge geometry is refined by a parameter allowing an ellipsoidal form. All in all, the shape is G2 (curvature) continuous and the parametric description possesses 14 degrees of freedom.

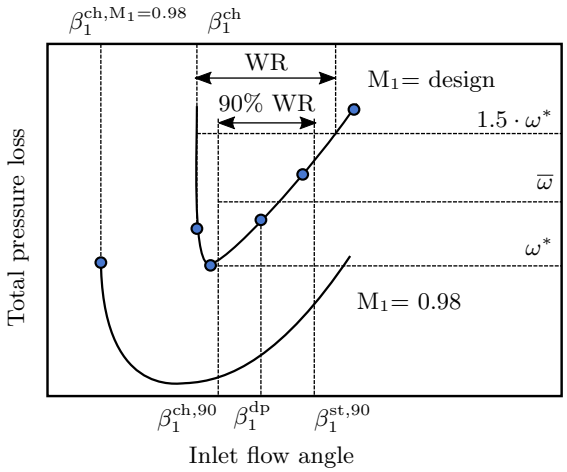

Figure 2: Definition of operating points for optimization

Blade-to-blade flow solver

All blade-to-blade calculations in the design work flow are carried out with the flow solver MISES developed at MIT [7]. The program discretizes the flow field with a coarse, two-dimensional grid on which the steady-state Euler equations are solved. These are coupled with the integral boundary layer equation into a single system of equations. Throughout the calculation procedure grid points are adjusted, until two edges of a computational cell coalesce with the flow's streamlines in a converged solution. Due to the inherent low grid resolution in comparison to a RANS setup, short computation times are achieved.

Quasi three-dimensional effects can be incorporated by prescribing stream tube thickness and radius. For this work, MVDR is modeled by a linearly contracting stream tube from leading to trailing edge. All computations are made with fully turbulent boundary layers.

The solver is well established among industry and research and it is validated to a high degree by experiments. A thorough analysis comparing wind tunnel tests and MISES is presented by Küsters et al. [5] for subsonic cascades. Their results show good agreement throughout the entire working range. Validation for transonic and supersonic inlet Mach numbers can be found in [8] and [9]. Reliability and speed make MISES a good choice for this work.

Numerical optimization

The actual airfoil design is performed with the multi-objective optimization suite "AutoOpti" [10, 11]. The optimizer has been developed at the DLR over the past 14 years with focus on application in turbomachinery. An evolutionary algorithm forms the basis of the design system and creates new candidates based on mutation and differential evolution. For each variation of the design parameters a process chain is evaluated to obtain the values of objective functions and constraints. Response surfaces are used in order to improve the selection of new candidates.

AIRFOIL DESIGN STRATEGY

This section proposes an optimization procedure for compressor airfoils. Throughout the development of this strategy, a set of 22 reference airfoils has been optimized repeatedly. After reviewing the results, the optimization process has been adapted until a satisfactory behavior was achieved for each airfoil. Both on-design and off-design behavior was considered, as well as geometric and structural feasibility. The reference airfoils have been selected to cover a wide range of requirements

that spans from airfoil sections of a fan over sections of a four stage transonic research compressor to a set of representative linear cascades.

In order to capture the essential performance characteristics of each candidate geometry, multiple operating points are evaluated. To design cascades at high subsonic inflow, the possibility of choke is accounted for. Throughout this optimization strategy the design requirements, as defined in the introduction, are fixed. The optimization parameters are formed by the airfoil shape parameters as presented above.

Operating points

The selection of operating points to evaluate off-design performance is crucial for the optimization result. At first, a strategy was implemented that uses a fixed number of five operating points (see [6]) with a difference in inflow angle computed based on an empirical correlation. At low inlet Mach numbers, resulting airfoil shapes achieved working ranges significantly wider than the correlation predicted. Correspondingly, the five operating points covered only parts of the actual working range, leaving potential for further improvement. Thus, in this work, both stall and choke branch of the loss characteristic are sampled with a variable number of operating points until the loss coefficient increases to 1.5 times minimum loss or choke occurs. The definition of operating points is shown in Fig. 2.

At first, the design point is determined by iteratively adjusting the back pressure until the desired design diffusion factor $\mathrm{DF}^{\mathrm{dp}}$ is reached. Using a good first approximation of the back pressure, a fixed number of three MISES evaluations is enough to get close to the target $\mathrm{DF}^{\mathrm{dp}}$. Afterwards, the inlet flow angle is increased iteratively using a fixed delta until the current loss is larger than 1.5 times design point loss. The delta in inlet flow angle is determined by correlations based on Lieblein [12] and Aungier [13]. Similarly, the choke point is found by decreasing the design point back pressure iteratively. The iteration loop terminates when either the cascade chokes or again the current loss is larger than 1.5 times design point loss. Choke detection is based on an automated analysis of the flow field.

The stall margin of the cascade is controlled by introducing an optimizer constraint that describes the relative distance of the design point to the stall limit:

$$(\beta_1^{\mathrm{st}} - \beta_1^{\mathrm{dp}})/\mathrm{WR} > 0.4. \tag{2}$$

When optimizing airfoils with supersonic inflow for many requirements airfoils result that choke due to unique incidence (see [14]). This shock system has low losses, but when reducing the inlet Mach number the cascade does no longer choke due to unique incidence, instead it chokes at the minimum cross section. This change in the shock system can put an upper limit to the mass throughput of the cascade. Both types of choking are depicted in Fig. 3 for an optimized transonic rotor tip section that is analyzed below. Against the background that high mass flow rates at part speed are desirable for stationary gas turbines, an operating point is computed that describes the mass throughput of the cascade for reduced inlet Mach numbers when the design inlet Mach number is supersonic. The additional operating point has an inlet Mach number slightly below unity (0.98) and the back pressure is chosen low enough so that the cascade chokes. At these inlet Mach numbers, choke typically occurs at the minimum cross section. It is desirable that the operating point at $\mathrm{M}_1 = 0.98$ has at least the same choke margin in comparison to the design point inlet Mach number. This is introduced as an additional constraint to the optimizer:

$$\beta_1^{\mathrm{ch,M_1=0.98}} - \beta_1^{\mathrm{ch}} < 0.5^\circ. \tag{3}$$

By allowing that the design point chokes at an angle 0.5° lower than the choke limit of the additional point, a certain degree of tolerance has been granted regarding this constraint.

When one of the MISES calculations does not converge, the corresponding candidate geometry is considered as “failed”.

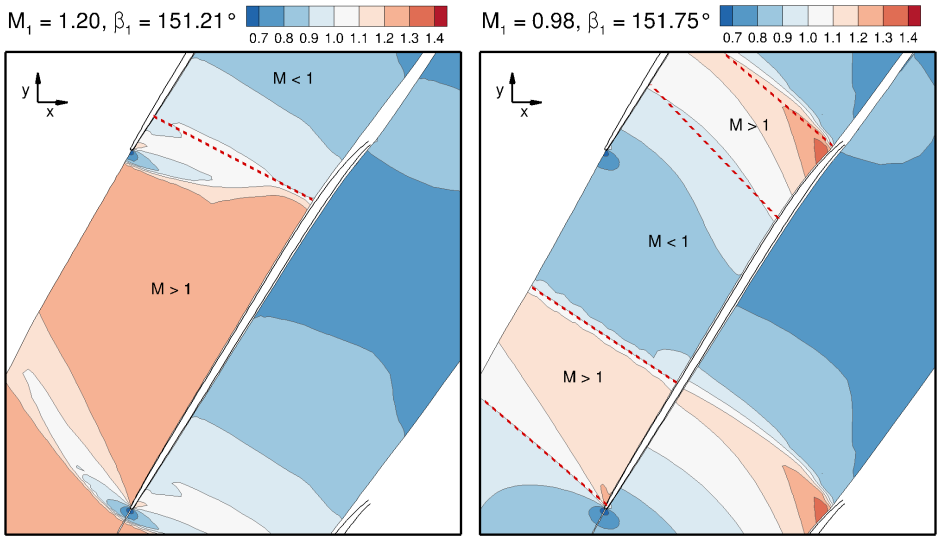

Figure 3: Mach number contours of transonic rotor tip cascade computed with MISES. Both operating points are choked at design inflow Mach number (left) and at an inlet Mach number close to sonic condition (right).

Objective function

After evaluating all operating points, the performance of the cascade has to be benchmarked. In general, the following objectives are desirable: low losses in design and off-design and a large working range. This typically constitutes a multi-objective optimization problem with a set of Pareto optimal solutions. For this work, only a single optimal solution is sought for a set of design requirements. Thus, a decision would have to be made after the optimization. Furthermore, it has to be considered that the working range is actually defined by the minimum loss. This makes it difficult to separate working range and level of losses as they are not directly conflicting due to their definition. For these two reasons, linear scalarization is applied to obtain a single objective function f with weights for the underlying objectives of the multi-objective optimization problem. f is composed of a set of weights multiplied with the objectives design point loss ω^{dp}, average total pressure loss $\overline{\omega}$ and working range WR:

$$f = \frac{0.2 \cdot \omega^{\mathrm{dp}} + 0.8 \cdot \overline{\omega}}{0.05} - \frac{\mathrm{WR}}{10°}. \tag{4}$$

The average total pressure loss is defined by an integration of loss over the range of inlet angles in a 90% working range:

$$\overline{\omega} = \frac{1}{\beta_1^{\mathrm{st},90} - \beta_1^{\mathrm{ch},90}} \int_{\beta_1^{\mathrm{ch},90}}^{\beta_1^{\mathrm{st},90}} \omega d\beta_1. \tag{5}$$

The integral is evaluated numerically by applying the trapezoidal rule to each pair of adjacent operating points. The selection of the weights in the objective function f is crucial for the optimization outcome. After manually tuning their values it was found that simply using fixed weights is sufficient to give satisfactory optimization results for each of the 22 reference airfoils.

Structural constraints

To assess the static and dynamic strength requirements of a blade, airfoil geometries have to be stacked and loading forces have to be applied. For an airfoil itself structural loading is not defined. Therefore, at least a set of heuristics in the form of constraints is introduced to assure structural integrity:

Table 1: Design requirements for the airfoils presented in this work

	M_1	$\frac{s}{c}$	γ	a	DF^{dp}	MVDR	Re
Transonic rotor mid	1.14	0.68	136.6°	2.8%	0.53	1.12	$2.5 \cdot 10^6$
Transonic rotor tip	1.20	0.82	147.1°	1.7%	0.50	1.12	$2.6 \cdot 10^6$
Subsonic stator	0.67	0.67	124.8°	4.5%	0.46	1.06	$1.2 \cdot 10^6$
Subsonic rotor mid	0.56	0.95	137.0°	5.1%	0.41	1.05	$1.0 \cdot 10^6$

- The desired airfoil's cross-sectional area is part of the design requirements and it is enforced with an optimizer constraint.
- The allowed minimum and maximum leading and trailing edge radii depend on the airfoil area.
- The axial position of the airfoil's center of area is limited to a value between 42.5% and 53.5% chord length.
- The curvature of the airfoil's thickness distribution is constrained to avoid concave parts in the thickness distributions. This prevents local minima in the thickness distribution and excessively slender blade shapes.

These constraints have an important influence on the optimization outcome and again they have been chosen based on the reference airfoils.

RESULTS I: TRANSONIC AIRFOILS

For subsonic airfoils the optimization is comparable to the strategy presented by Köller [4]. Thus, only a closer look to optimization results for supersonic inflow is taken at this point. Further evaluations for two subsonic airfoils can be found below. A mid and tip section taken from the first rotor of the research compressor DLR-Rig250 [15] is examined in comparison to versions optimized with the presented design work flow. The requirements of these airfoil sections are given in Tab. 1 and the geometric and aerodynamic evaluations in Fig. 4. The flow field of the optimized transonic rotor tip section is depicted in Fig. 3. Design work flows based on MISES in combination with numerical optimization are not as validated for supersonic inflow as they are for subsonic inflow. For this reason, a comparison of the MISES results to computations with a steady-state RANS solver is drawn here as well.

At first, the baseline and optimized versions are compared with focus on the results computed by MISES. The optimized versions of both airfoils share many similarities. Looking at the loss and outflow angle characteristics, the optimized airfoils choke at lower inflow angles and achieve significantly lower losses in this region in comparison to the baseline designs. The minimum total pressure loss of both airfoils is reduced by approximately 0.02. The design points move to lower inflow angles as well. Accordingly, to maintain the same design point diffusion, the outflow angle reduces in comparison to the baseline designs. For positive incidence, the new airfoils show similar losses than the baseline designs.

When analyzing the isentropic Mach number distribution of the design points it can be observed how the suction side curvature controls the velocities upstream of the shock. As the development of suction side curvature shows, both optimized airfoils show a short region with a concave curvature upstream of the passage shock. This so-called pre-compression decelerates the velocity isentropically, reducing the pre-shock Mach number to minimize shock losses. The optimized tip airfoil has an inflow Mach number of 1.20 and maintains a isentropic Mach number between 1.26 and 1.28 from 10% to 40% chord length. Just upstream of the shock, the isentropic Mach number is reduced to a pre-shock Mach number of 1.23 and the shock occurs at a chord length of 70%. In comparison, the baseline design has a higher pre-shock

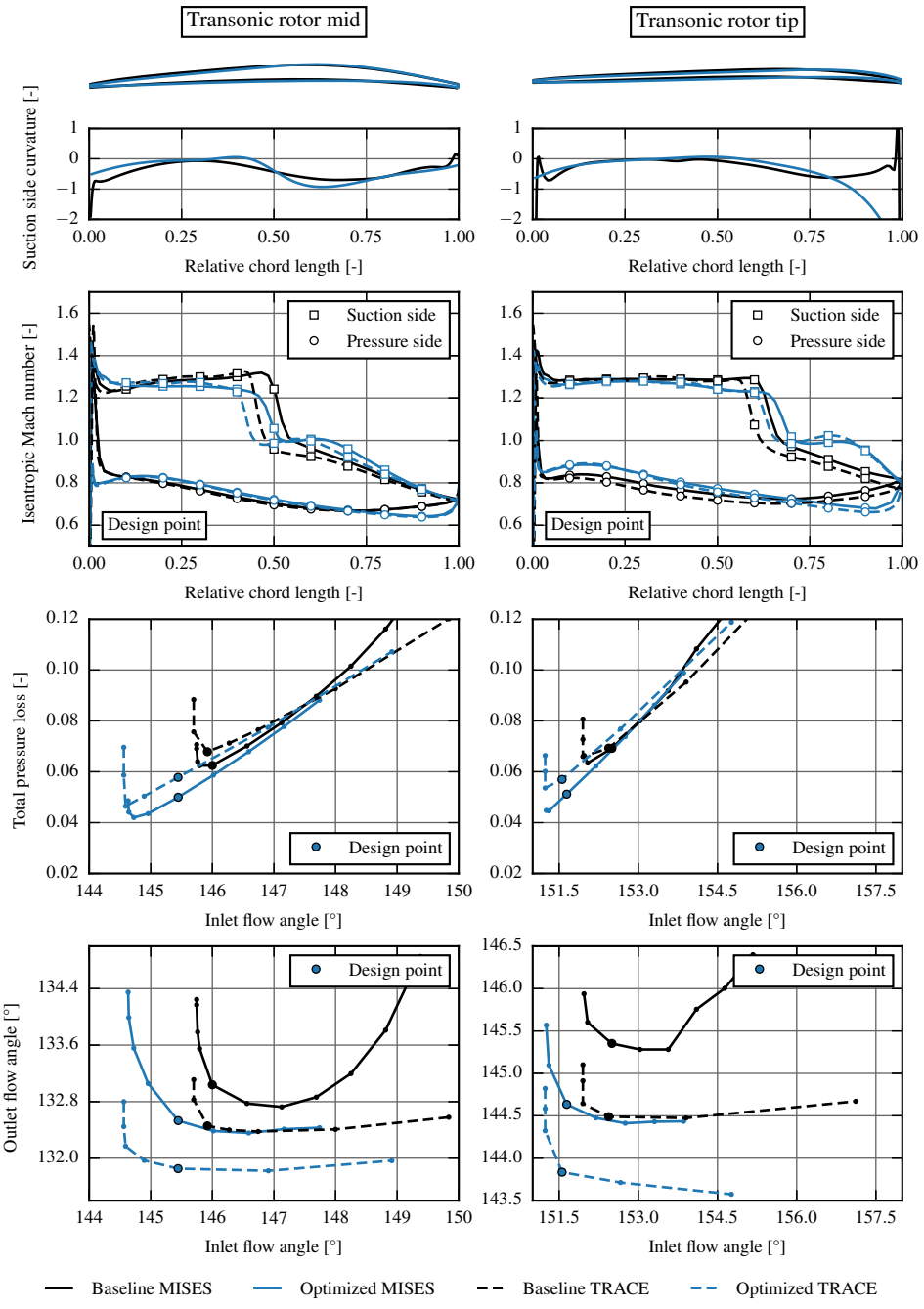

Figure 4: Airfoil geometry, computed isentropic Mach number and loss characteristic for two transonic rotor airfoils comparing MISES and TRACE results

Table 2: Upper and lower limits for database design requirements

	M_1	$\frac{s}{c}$	γ	a	DF^{dp}	MVDR	Re
Lower	0.35	0.50	110.0°	1.5%	0.35	1.0	$5 \cdot 10^5$
Upper	1.20	1.20	147.5°	8.5%	0.55	1.2	$5 \cdot 10^6$

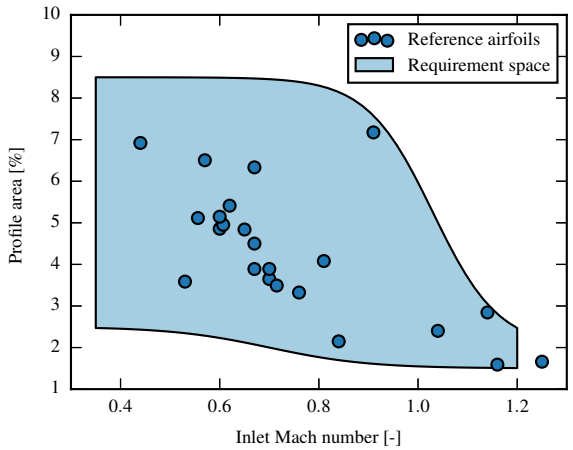

Figure 5: Minimum and maximum profile area of the airfoil family depending on the design inlet Mach number and locations of the reference airfoils

Mach number of 1.29. Another important geometric modification that influences the loss is a smaller leading edge radius. This reduces the strength of the bow shock, but it has to be considered that the blade becomes more vulnerable to erosion.

These results are now assessed by simulations carried out with the flow solver TRACE [16] using a steady-state RANS setup with a k-ω turbulence model and a low-Reynolds wall treatment assuming fully turbulent boundary layers. The MVDR is modeled with contracting inviscid walls. The choke limits can be confirmed very well. In all cases, TRACE predicts higher losses in the design region than MISES. Differences increase for the optimized versions. This indicates that the optimizer exploits effects that are not reproduced by TRACE. Furthermore, TRACE shows lower outflow angles and a smaller increment of deviation for higher incidences. Although the quantitative results show deviations, TRACE confirms the qualitative trends shown by the optimized airfoils. These results qualify MISES as a tool for the design of airfoils at supersonic inflow.

AIRFOIL DATABASE

The optimization strategy is now applied to a large set of design requirements. The optimization results are stored in a relational database including optimal geometries, MISES calculations and information about the optimization progress. Furthermore, for each optimal airfoil, specific loss and deviation correlations are fitted with methods described in [17]. The database is implemented as a relational SQL database [18] running on a central server.

Requirement space

The design requirements presented in the introduction form a seven dimensional space. Adding a lower and upper bound for each parameter with values given in Tab. 2, a seven dimensional hyper-rectangle is obtained. This definition of the requirement space contains large regions that either do not occur in compressor

design or are actually infeasible. For example, the hyper-rectangle includes thick blades at high inlet Mach numbers. As high inlet Mach numbers occur only in the upper part of rotors where blade thickness is already reduced, this region is of no interest. Accordingly, five constraints limiting the requirement space are introduced:

- A minimum and maximum profile area dependent on the inlet Mach number, see Fig. 5,
- A lower limit for an approximation of the cascade throat,
- A lower limit for the overlapping of two adjacent airfoils to ensure that a passage is formed,
- An upper and lower limit of the blade stagger angle dependent on the inlet Mach number in order to control the axial inlet Mach number,
- An upper limit for profile area dependent on the stagger angle, as thick airfoils are in the hub region with low stagger angles.

Each of these constraints connects two or three requirements and they can be evaluated directly without having to optimize an airfoil. These limits have been determined based on the mentioned reference airfoils and additional blade sections from a multi-stage axial compressor.

The lower limit of the stagger angle represents a major limitation of the database. It might exclude requirements of outlet guide vanes and rotor hub sections of fans with high bypass ratios. Furthermore, the requirements for inlet guide vanes are not included in the database at all. These applications are very specific and should be handled by additional variations in the corresponding regions of interest.

Creation

All in all, 2048 optimizations have been carried out at discrete points in the requirement space. In comparison, Köller [4] obtained 411 optimal profile geometries in his work. In order to achieve a uniform distribution of the airfoils in the requirement space, a space filling design is used. Here, the maximum entropy strategy is chosen, which minimizes the correlation between samples [19]. The idea of the sampling strategy can be compared to maximizing the minimum distance between two arbitrary samples.

The optimizations have been launched in five batches. From one batch to the next the airfoils from previous batches have been used to initialize the optimizations. In each optimization, an average of 4800 airfoils are evaluated. The optimizations are terminated when the improvement over 500 successful candidates becomes insignificant or an evaluation limit is reached. The evaluation of the whole process chain for new candidates was successful in only 38% of the cases. Particularly for high inlet Mach numbers or operating points with high incidence MISES evaluations fail often. For 31 requirement sets, no airfoil was found fulfilling the optimizer constraints, this corresponds to 1.5% of all requirement sets. The whole computation time that was spend on the 2048 optimizations comes down to 85 000 CPU hours on current hardware.

Interpolation

Optimal airfoils are now defined on discrete points in the requirement space and interpolation routines can be used to create airfoils at locations in-between. Here, the interpolation function is used to approximate blade shape parameters for a new set of design requirements. Afterwards, the program “BladeGenerator” can be executed to obtain the profile surface. The interpolation problem comes down to

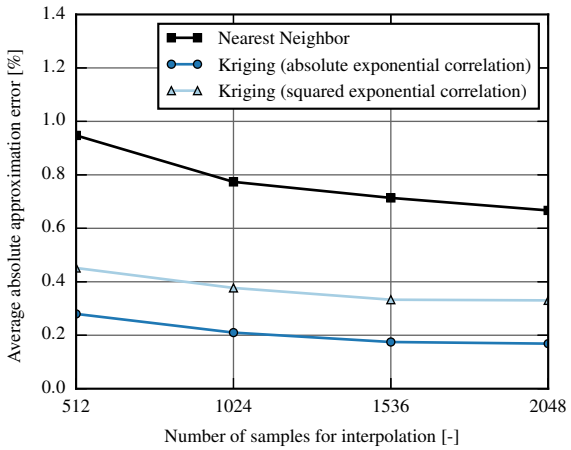

Figure 6: Average absolute approximation error of profile area for 10,000 random sets of requirements over the number of samples used for interpolation

multivariate interpolation of scattered data on an irregular grid. Multiple interpolation methods have been compared, among them is nearest neighbor interpolation and Kriging [20].

A simple metric to determine the quality of an interpolation routine is the difference between the desired profile area from the design requirements and the obtained profile area computed by the airfoil shape. This approximation error can be evaluated for arbitrary design requirements without having to optimize the corresponding optimal airfoil shape. Fig. 6 depicts this metric for the interpolation routines under investigation and different sizes of interpolation samples. The approximation error is averaged over 10,000 random samples in the requirement space. It can be observed how the approximation error decreases for an increment in sample size. The higher the number of samples gets, the lower is the benefit of adding additional samples. Based on this analysis it was decided that it is not necessary to optimize more airfoils for the database. In the end, Kriging with an absolute exponential correlation has the lowest approximation error and is chosen to interpolate new airfoil shapes. Using the interpolation, approximations for optimal airfoil shapes can be generated in fractions of a second.

RESULTS II: INTERPOLATED AIRFOILS

In order to assess the quality of interpolated profile shapes, two further representative airfoils are evaluated. For both cases, a baseline design is compared to an airfoil interpolated from the database and a geometry that was subsequently optimized. This way, it is possible to assess how close the interpolated airfoils are to the results of the optimization strategy. It is important to notice that the reference airfoils are not included in the database. The geometries, isentropic Mach number distributions and loss characteristics are displayed in Fig. 7. To the left, a subsonic stator section of stage four of DLR-Rig250 [15] is analyzed. To the right, one of the optimized airfoils published by Köller (test cascade C in [4]) is compared to the results of this work. The design requirements of the cascades are found in Tab. 1.

Comparing the geometry of the baseline and of the optimized stator airfoil (left side), the maximum thickness moves closer to the leading edge from about 40% to 25% relative chord. Together with the blade thickness, the camber as well as the suction side curvature increases in the front part. This leads a higher suction side maximum velocity which moves upstream from 20% to 10% relative chord. 90% of the blade suction side can now be used for flow deceleration. At

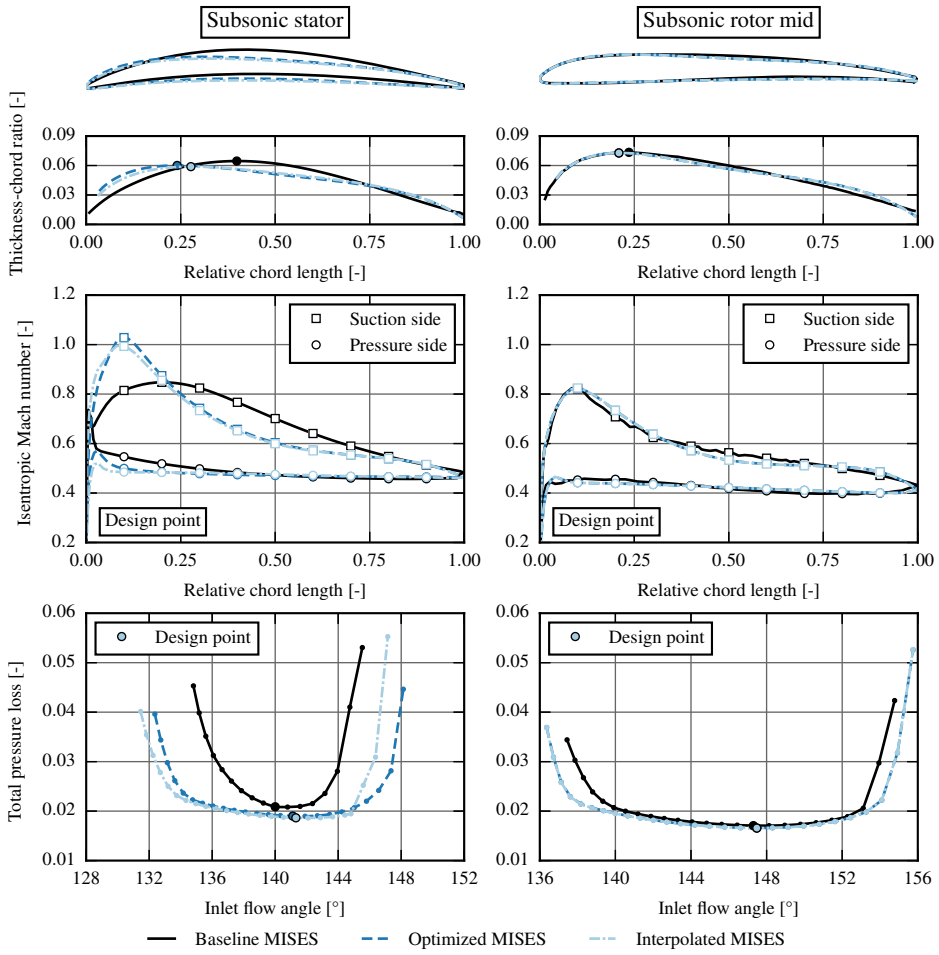

Figure 7: Airfoil geometry, computed isentropic Mach number and loss characteristic for two subsonic airfoils comparing the baseline design, a design interpolated from the presented database and a design that was subsequently optimized

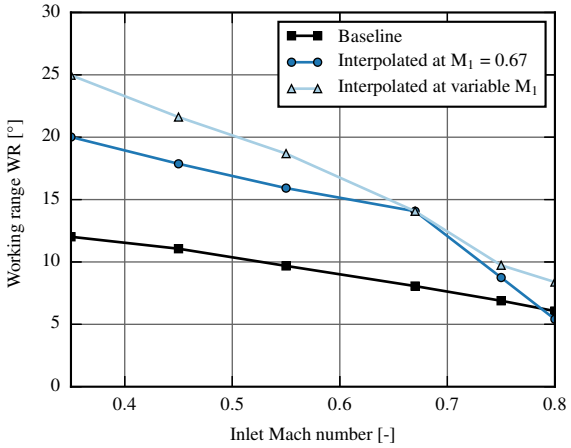

Figure 8: Working range over inlet Mach number for the subsonic stator profile (see Tab. 1). Baseline geometry is compared to airfoil at a design Mach number of 0.67 and airfoils chosen for each Mach number

first, with an intact boundary layer, a strong diffusion is observed. In the middle and rear of the blade the diffusion is low. Furthermore, the leading edge radius increases. This offers a high robustness towards incidence variation improving off-design performance. Although the interpolated and the subsequently optimized geometries are close to each other and show similar aerodynamics, a significant difference in performance can be seen for the stall branch of the loss characteristic. This highlights the importance of the interpolation routines.

The optimization strategy of this paper is validated by the optimal airfoil shapes that are published by Köller [4]. Here, a comparison to one of the design tasks is drawn (right side). For this set of requirements, the interpolation from the database gives an excellent result and no further improvement was possible in the subsequent optimization. Accordingly, a differentiation between interpolated and optimized airfoil does not have to be performed. Overall, the new profile resembles the design by Köller and the flow characteristics are similar to the ones already observed in the stator cascade. In comparison to the baseline design by Köller, the location and the value of the maximum suction side velocity in the design point did not change. But, for the new airfoils, hardly any flow deceleration is observed between 60% and 70% relative chord. This is even less than the baseline design shows. Regarding the pressure side, for each design the velocity distribution is almost constant. The flow characteristics that Köller discussed seem to be more pronounced for the new airfoils. A possible reason is that in this work the geometric parameterization has more degrees of freedom. The working range and losses improved to some extend as well.

One question that remains is if the benefit of having airfoils optimized for a specific purpose is large enough to justify the effort of optimizing hundreds of airfoils. To study this, Fig. 8 analysis the working range of the subsonic stator airfoil over the inlet Mach number. The baseline design is compared to a database airfoil that was selected at a design Mach number of 0.67 and furthermore for each inlet Mach number an airfoil was interpolated that is specifically designed for it. At the design Mach number of 0.67, the optimized airfoils have a working range of 14 degree in comparison to 7 degree for the baseline geometry. The baseline airfoil shows a nearly linear behavior of working range over inlet Mach number. At low Mach numbers, the baseline profile has an incidence range of 12 degree. The airfoil that is actually optimized for an inlet Mach number of 0.67 still offers 8 degree additional working range. The largest working range of 25 degree is supplied by the airfoil specifically optimized for low Mach numbers. This is twice the working range that the baseline airfoil shows. For high Mach

numbers, the airfoil optimized for an inlet Mach number of 0.67 suddenly looses working range due to a shock that forms in the cambered front part of the blade. When interpolating new blades, the working range drops as well. Still, for an inlet Mach number of 0.8 the database airfoil possesses almost 40% more working range than the baseline design. Consequently, it can be said that the database airfoils show superior performance in the regions they are designed for. But, care has to be taken when database airfoils are not applied correctly or the compressor is running at over speed. In this case, standard airfoils can outperform the database airfoils.

CONCLUSION

The major result of this work is a functional relation between a set of design requirements and a corresponding optimal airfoil shape that can be evaluated in fractions of a second. The approach is based on a design strategy for compressor airfoils. It uses numerical optimization and computes the loss characteristics of candidate airfoils around the design point with MISES. On this basis, a database of optimal airfoils is generated and interpolation routines are employed to receive new airfoil geometries.

Most requirements for the design of multi-stage axial compressors are covered by this database: from transonic front to subsonic rear stages, from thick hub to slender tip blade sections. For all these requirements an optimal airfoil shape can be found with the presented methods. In order to validate the design strategy, the performance of two transonic cascades is analyzed with RANS. For two subsonic cases, new airfoils are compared to a controlled diffusion airfoil and a state-of-the-art stationary gas turbine airfoil. The new airfoils achieve larger working ranges and lower losses.

In addition to the presented methods, loss and deviation correlations have been derived for the new airfoils with methods presented in [17]. These can now be used for compressor design with throughflow codes. Based on the stagger angle, the desired aerodynamic loading, the airfoil's cross-section area and the current flow condition, the requirements to access the airfoil database are determined and a blade geometry can be generated. Work flows are implemented to access the database in throughflow as well as 3D CFD compressor design.

A full assessment of the new airfoils is hard when examining only a few airfoils, as it was done in this work. For this reason, the next step is to further validate the airfoils by applying them throughout the design of a multi-stage axial compressor. Afterwards, the database will be used to study novel concepts for aircraft engines.

REFERENCES

[1] Lieblein, S., and Johnsen, I., 1961. "Resume of Transonic-Compressor Research at NACA Lewis Laboratory". *ASME J. Eng. Power.,* ***83***(3), pp. 219–232.

[2] Johnsen, I., and Bullock, R., 1965. Aerodynamical Design of Axial-Flow Compressors. Tech. Rep. NASA-SP-36, NASA Lewis Research Center, Cleveland, OH, United States.

[3] Hobbs, D., and Weingold, H., 1984. "Development of Controlled Diffusion Airfoils for Multistage Compressor Application". *ASME J. Eng. Gas Turbines Power,* ***106***(2), pp. 271–278.

[4] Köller, U., Mönig, R., Küsters, B., and Schreiber, H.-A., 2000. "Development of Advanced Compressor Airfoils for Heavy-Duty Gas Turbines - Part I: Design and Optimization". *ASME J. Turbomach,* ***122***(3), pp. 397–405.

[5] Küsters, B., Schreiber, H.-A., Köller, U., and Mönig, R., 2000. "Development of Advanced Compressor Airfoils for Heavy-Duty Gas Turbines - Part II:

Experimental and Theoretical Analysis". *ASME J. Turbomach,* ***122***(3), pp. 406–414.

[6] Schnoes, M., and Nicke, E., 2017. "A Database of Optimal Airfoils for Axial Compressor Throughflow Design". *ASME J. Turbomach,* ***139***(5), p. 051008.

[7] Drela, M., and Youngren, H., 1998. *A User's Guide to MISES 2.53.* MIT Aerospace Computational Design Laboratory, Cambridge, MA, United States.

[8] Youngren, H., 1991. Analysis and design of transonic cascades with splitter vanes. Tech. Rep. Report 203, Gas Turbine Laboratory, Massachusetts Institute of Technology, Cambridge, MA, United States.

[9] Fuchs, R., Schreiber, H. A., Steinert, W., and Küsters, B., 1998. "Ein verlustminimiertes Verdichtergitter für einen transsonischen Rotor - Entwurf und Analyse". *VDI-Berichte*(1425), pp. 259–270.

[10] Aulich, M., Voss, C., and Raitor, T., 2014. "Optimization Strategies demonstrated on a Transonic Centrifugal Compressor". *ISROMAC 15.*

[11] Voss, C., Aulich, M., and Raitor, T., 2014. "Metamodel Assisted Aeromechanical Optimization of a Transonic Centrifugal Compressor". *ISROMAC 15.*

[12] Lieblein, S., 1957. Analysis of experimental low-speed loss and stall characteristics of two-dimensional compressor blade cascades. Tech. Rep. NACA-RM-E57A28, National Advisory Committee for Aeronautics. Lewis Flight Propulsion Lab., Cleveland, OH, United States.

[13] Aungier, R. H., 2003. *Axial-Flow Compressors.* ASME Press.

[14] Cumpsty, N. A., 2004. *Compressor Aerodynamics.* Krieger Pub Co.

[15] Schönweitz, D., Voges, M., Goinis, G., Enders, G., and Johann, E., 2013. "Experimental and Numerical Examinations of a Transonic Compressor-Stage With Casing Treatment". *ASME Paper No. GT2013-95550.*

[16] Becker, K., Heitkamp, K., and Kügeler, E., 2010. "Recent Progress in a Hybrid-Grid CFD Solver for Turbomachinery Flows". *ECCOMAS CFD 2010.*

[17] Schnoes, M., and Nicke, E., 2015. "Automated Calibration of Compressor Loss and Deviation Correlations". *ASME Paper No. GT2015-42644.*

[18] Widenius, M., and Axmark, D., 2002. *Mysql Reference Manual*, 1st ed. O'Reilly & Associates, Inc., Sebastopol, CA, USA.

[19] Shewry, M. C., and Wynn, H. P., 1987. "Maximum entropy sampling". *Journal of Applied Statistics,* ***14***(2), p. 165–170.

[20] Lophaven, S. N., Nielsen, H. B., and Søndergaard, J., 2002. DACE - a matlab kriging toolbox, version 2.0. Tech. rep., Informatics and Mathematical Modelling, Technical University of Denmark, DTU.

APPENDIX

Table 3: Transonic rotor mid

suction side		pressure side	
x	y	x	y
0.000000	0.000000	0.000000	0.000000
0.000794	0.001338	0.001024	-0.001164
0.002136	0.002226	0.002505	-0.001781
0.003608	0.002879	0.004070	-0.002140
0.005151	0.003344	0.005668	-0.002301
0.006734	0.003644	0.007275	-0.002292
0.008328	0.003879	0.008877	-0.002218
0.009924	0.004113	0.010486	-0.002144
0.012059	0.004423	0.012634	-0.002045
0.014918	0.004834	0.015507	-0.001913
0.018745	0.005375	0.019352	-0.001738
0.023870	0.006086	0.024495	-0.001505
0.030733	0.007017	0.031377	-0.001197
0.039924	0.008228	0.040584	-0.000789
0.052232	0.009795	0.052902	-0.000252
0.068717	0.011812	0.069382	0.000452
0.090797	0.014393	0.091432	0.001369
0.120369	0.017680	0.120933	0.002553
0.159976	0.021856	0.160404	0.004067
0.213020	0.027160	0.213217	0.005963
0.284050	0.033943	0.283880	0.008263
0.379146	0.042784	0.378433	0.010890
0.506441	0.054515	0.504954	0.013465
0.633835	0.059184	0.631197	0.014652
0.728467	0.053429	0.725119	0.014277
0.798422	0.044589	0.794980	0.012979
0.850159	0.036064	0.846931	0.011193
0.888474	0.028834	0.885552	0.009211
0.916882	0.023037	0.914253	0.007228
0.937963	0.018519	0.935575	0.005363
0.953615	0.015050	0.951410	0.003687
0.965241	0.012412	0.963166	0.002233
0.973878	0.010418	0.971893	0.001006
0.980297	0.008918	0.978371	-0.000004
0.985067	0.007794	0.983179	-0.000820
0.988614	0.006952	0.986750	-0.001467
0.991254	0.006322	0.989401	-0.001973
0.993215	0.005854	0.991371	-0.002365
0.994676	0.005504	0.992834	-0.002666
0.996131	0.005156	0.994296	-0.002974
0.997580	0.004802	0.994296	-0.002974
0.998924	0.004164	0.997241	-0.003271
0.999780	0.002952	0.998529	-0.002541
1.000113	0.001498	0.999455	-0.001377
0.999998	0.000009	0.999998	0.000009

Table 4: Transonic rotor tip

suction side		pressure side	
x	y	x	y
0.000928	0.001317	0.000928	0.001317
0.002367	0.002149	0.000000	0.000000
0.003924	0.002737	0.000986	-0.001259
0.005542	0.003128	0.002492	-0.001957
0.007193	0.003345	0.004100	-0.002382
0.008850	0.003503	0.005749	-0.002596
0.010509	0.003660	0.007412	-0.002636
0.012724	0.003867	0.009067	-0.002631
0.015683	0.004137	0.010737	-0.002626
0.019636	0.004488	0.012961	-0.002619
0.024918	0.004941	0.015928	-0.002609
0.031975	0.005520	0.019889	-0.002594
0.041405	0.006251	0.025178	-0.002571
0.054005	0.007162	0.032240	-0.002536
0.070842	0.008277	0.041670	-0.002482
0.093341	0.009616	0.054261	-0.002396
0.123404	0.011191	0.071073	-0.002258
0.163574	0.013015	0.093521	-0.002036
0.217243	0.015100	0.123493	-0.001675
0.288943	0.017523	0.163513	-0.001088
0.384719	0.020544	0.216947	-0.000142
0.512636	0.024959	0.288289	0.001362
0.639812	0.029892	0.383542	0.003686
0.733997	0.032206	0.510722	0.007030
0.803737	0.031916	0.637193	0.010081
0.855319	0.029798	0.730861	0.011621
0.893408	0.026683	0.800232	0.011913
0.921486	0.023229	0.851599	0.011300
0.942155	0.019855	0.889620	0.010098
0.957356	0.016808	0.917747	0.008565
0.968533	0.014204	0.938541	0.006899
0.976752	0.012056	0.953898	0.005241
0.982800	0.010330	0.965230	0.003685
0.987252	0.008969	0.973585	0.002290
0.990532	0.007911	0.979740	0.001081
0.992951	0.007099	0.984273	0.000066
0.994736	0.006480	0.987610	-0.000766
0.996056	0.006015	0.990068	-0.001433
0.997372	0.005550	0.991880	-0.001960
0.998657	0.005005	0.993215	-0.002369
0.999667	0.004059	0.993215	-0.002369
1.000181	0.002767	0.995895	-0.003148
1.000273	0.001377	0.997269	-0.003002
0.999999	0.000010	0.998457	-0.002282
0.999377	-0.001237	0.999377	-0.001237

Table 5: Subsonic stator

suction side		pressure side	
x	y	x	y
0.001851	0.007342	0.001851	0.007342
0.007178	0.013257	0.000000	0.000000
0.013227	0.018447	0.006899	-0.003616
0.019663	0.023150	0.014821	-0.004602
0.026378	0.027446	0.022810	-0.004673
0.033266	0.031459	0.030783	-0.004144
0.040292	0.035226	0.038711	-0.003144
0.049373	0.039648	0.046600	-0.001872
0.061114	0.044737	0.054493	-0.000612
0.076288	0.050447	0.064468	0.000912
0.095876	0.056631	0.077079	0.002734
0.121104	0.063022	0.093025	0.004883
0.153487	0.069228	0.113188	0.007369
0.194906	0.074670	0.138688	0.010168
0.247691	0.078576	0.170938	0.013204
0.314737	0.080065	0.211720	0.016324
0.399685	0.078212	0.263284	0.019238
0.507181	0.072308	0.328458	0.021491
0.614235	0.064372	0.410797	0.022433
0.698112	0.056605	0.514766	0.021183
0.763796	0.049192	0.618317	0.017858
0.815206	0.042302	0.699695	0.014167
0.855426	0.036049	0.763658	0.010789
0.886881	0.030504	0.813939	0.007931
0.911476	0.025684	0.853470	0.005608
0.930707	0.021561	0.884550	0.003758
0.945743	0.018082	0.908988	0.002304
0.957503	0.015186	0.928204	0.001167
0.966702	0.012801	0.943313	0.000281
0.973901	0.010854	0.955193	-0.000409
0.979535	0.009274	0.964535	-0.000946
0.983947	0.008000	0.971880	-0.001365
0.987403	0.006978	0.977655	-0.001691
0.990110	0.006161	0.982197	-0.001946
0.992231	0.005510	0.985767	-0.002146
0.993894	0.004993	0.988575	-0.002302
0.995198	0.004584	0.990783	-0.002424
0.996223	0.004260	0.992518	-0.002520
0.997243	0.003938	0.993883	-0.002595
0.998253	0.003583	0.994956	-0.002654
0.999137	0.002988	0.994956	-0.002654
0.999732	0.002103	0.997104	-0.002733
1.000021	0.001075	0.998143	-0.002488
0.999998	0.000007	0.999015	-0.001869
0.999648	-0.001005	0.999648	-0.001005

Table 6: Subsonic rotor mid

suction side		pressure side	
x	y	x	y
0.001811	0.009049	0.001811	0.009049
0.008449	0.016159	0.000000	0.000000
0.016101	0.022192	0.007956	-0.005399
0.024256	0.027528	0.017388	-0.007991
0.032760	0.032291	0.027062	-0.009488
0.041491	0.036626	0.036823	-0.010242
0.050411	0.040557	0.046613	-0.010366
0.061660	0.044888	0.056399	-0.010064
0.075831	0.049518	0.066186	-0.009721
0.093645	0.054261	0.078244	-0.009311
0.115980	0.058838	0.093102	-0.008823
0.143880	0.062902	0.111411	-0.008243
0.178609	0.066015	0.133971	-0.007555
0.221699	0.067687	0.161769	-0.006742
0.275030	0.067494	0.196023	-0.005786
0.340945	0.065215	0.238231	-0.004670
0.422409	0.061097	0.290240	-0.003382
0.523172	0.056401	0.354327	-0.001925
0.622979	0.052643	0.433296	-0.000329
0.702073	0.049089	0.530606	0.001308
0.764710	0.045150	0.626888	0.002499
0.814276	0.040845	0.703381	0.003057
0.853460	0.036373	0.764151	0.003175
0.884411	0.031961	0.812428	0.002997
0.908841	0.027787	0.850780	0.002627
0.928111	0.023963	0.881245	0.002141
0.943307	0.020550	0.905445	0.001597
0.955290	0.017577	0.924666	0.001035
0.964740	0.015032	0.939933	0.000484
0.972195	0.012886	0.952058	-0.000036
0.978079	0.011094	0.961687	-0.000515
0.982723	0.009612	0.969335	-0.000944
0.986392	0.008396	0.975408	-0.001323
0.989291	0.007405	0.980231	-0.001651
0.991582	0.006600	0.984061	-0.001931
0.993394	0.005950	0.987102	-0.002168
0.994829	0.005427	0.989518	-0.002366
0.995967	0.005009	0.991437	-0.002530
0.997100	0.004593	0.992960	-0.002665
0.998218	0.004135	0.994171	-0.002775
0.999179	0.003413	0.994171	-0.002775
0.999804	0.002384	0.996593	-0.002958
1.000078	0.001210	0.997777	-0.002721
0.999998	0.000008	0.998790	-0.002060
0.999549	-0.001116	0.999549	-0.001116